Available online at www.sciencedirect.com

ScienceDirect

Ceramics International 40 (2014) 4521–4527

CERAMICS INTERNATIONAL

www.elsevier.com/locate/ceramint

Temperature induced evolution of structure/microstructure parameters and their correlations with electric/magnetic properties of nanocrystalline Nickel ferrite

Milica Vucinic-Vasic[a,*], Marko Boskovic[b], Aleksandar Antic[a], Goran Stojanovic[a], Milan Radovanovic[a], Martin Fabian[c], Cedomir Jovalekic[d], Miodrag B. Pavlovic[e], Bratislav Antic[b]

[a]Faculty of Technical Sciences, University of Novi Sad, Trg D. Obradovica 6, 21000 Novi Sad, Serbia
[b]The "Vinča" Institute of Nuclear Sciences, University of Belgrade, P.O. Box 522, 11001 Belgrade, Serbia
[c]Institute of Geotechnics, Slovak Academy of Sciences, 043 53 Košice, Slovakia
[d]Insitute for Multidisciplinary Studies, University of Belgrade, Kneza Viseslava 1, 11001 Belgrade, Serbia
[e]Faculty of Electrical Engineering, University of Belgrade, POB 3554, 11000, Belgrade, Serbia

Received 22 May 2013; received in revised form 25 August 2013; accepted 29 August 2013
Available online 7 September 2013

Abstract

Nickel ferrite nanoparticles were annealed in order to find dependence of electric/magnetic properties on crystallite size. The following correlations of crystallite size with physical parameters were found: (a) lattice parameter decreases with the increase in size and it reaches value for bulk counterpart approximately for crystallites bigger than 7 nm, (b) ac electrical resistivity at room temperature increases with the increase in crystallite size, (c) for crystallites of ~7 nm or smaller electrical resistivity have maximum value at 50 °C, (d) the real part of permittivity at selected frequency generally decreases with the increase in crystallite size and (e) magnetization increases with the increase in crystallite size. Deviation of stoichiometry, cation polyvalence, and cation redistribution with annealing are the main factors that influence physical properties of Nickel ferrite nanoparticles.

Keywords: B. Grain size; C. Electrical properties; C. Magnetic properties; D. Ferrite

1. Introduction

For years now, ferrites in the form of nano powders and thin films have been arousing great interest in scientific community. The reason is their applicability in modern technology and the fact that they often serve as modal systems in the research of new phenomena in basic sciences. It is well known that properties of materials at nano scale depend on a number of factors such as composition, shape, size, surface morphology, anisotropy, inter-particle interactions, etc. [1]. Ferrites with spinel structure are traditionally divided into two different ideal types of structures, normal and inverse. Normal spinel ferrites are described by the formula $(M)[Fe]_2O_4$, where (M) and [Fe] represent the tetrahedral and octahedral sites occupied by metal and iron ions, respectively. Bulk $NiFe_2O_4$ has an inverse spinel structure with Ni^{2+} ions occupying half of the octahedral sites and Fe^{3+} ions occupying tetrahedral and half of the octahedral sites $(Fe)[NiFe]_2O_4$. Mixed spinel structure, with Ni^{2+} ions distributed in both tetrahedral and octahedral sites in different ratio, was found for nanocrystalline $NiFe_2O_4$ [2,3].

Electrical and magnetic properties of nanocrystalline ferrites depend on the nature of the ions, their charges and their distribution between tetrahedral and octahedral sites, as well as on microstructure parameters – predominantly on crystallite size. The main mechanism of conductivity in spinels is hopping of electrons among cations in different valence states distributed over octahedral 16d sites [4]. Stoichiometric nickel ferrite is generalized as Mott insulator modal system [5]. There are papers reporting some deviation from stoichiometry [6] and, on the other hand there are papers claiming formation of stoichiometric nanosized nickel ferrite [7]. However, it is doubtful

*Corresponding author. Tel./fax: +381 21635 0770.
E-mail address: milicavv@uns.ac.rs (M. Vucinic-Vasic).

0272-8842/$ - see front matter © 2013 Elsevier Ltd and Techna Group S.r.l. All rights reserved.
http://dx.doi.org/10.1016/j.ceramint.2013.08.127

whether a nanosized stoichiometric nickel ferrite can be produced. It is known that the electrical properties of bulk $NiFe_2O_4$ are closely related to a small deficiency of oxygen [8]. Deviation from stoichiometry results in polyvalence of iron ions (+2, +3) which leads to a marked lowering of activation energy of conduction electrons [8], and the resistivity of nickel ferrites therefore depends on the concentration of ferrous (Fe^{2+}) ions. From magnetic point of view, properties of nanomaterials are significantly modified in comparison with the bulk counterparts. Depending on the particle size, Ni-ferrite can exhibit ferrimagnetism, superparamagnetism or paramagnetism [9,10]. Ni-ferrite nanoparticles with size above 15 nm and bulk counterpart show ferrimagnetism, while smaller nanoparticles are superparamagnetic. Paramagnetism is found in noncrystalline Ni-ferrites [9,10].

It is known that synthesis procedure determines structural and microstructural characteristics of materials. Hence, there are numerous papers oriented toward development of new procedures and the improvement of existing ones [11]. Lazarevic at al. reported soft mechanochemical synthesis of Nickel ferrite nanoparticles using hydroxides and carbonates as starting compounds [12]. One of the Nickel ferrite samples investigated by Lazarevic at al. [12] was selected and used in present research. In order to obtain samples with different crystallite size, as-prepared sample was annealed at 300, 500 and 700 °C.

The objective of this work was to determine microstructure of nickel ferrite nanoparticles by combining X-ray diffraction line broadening analysis and transmission electron microscopy method, and afterwards to find relations between microstructure and, structural, electric and magnetic properties.

2. Experimental

High energy ball milling (HEBM) was used for preparation of Nickel ferrite nanoparticles. Mixtures of crystalline powders, $Ni(OH)_2$ and $Fe(OH)_3$, were milled in air atmosphere in planetary ball mill (Fritsch Pulverisette 5). A hardened-steel vial of 500 cm^3 volume, filled with 40 hardened steel balls with a diameter of 13.4 mm, was used as the milling medium. The mass of the powder was 20 g and the balls-to-powder mass ratio was 20:1 [12]. As-prepared sample (S0) was annealed at 300, 500 and 700 °C for 3 h. The obtained samples were denoted S300, S500 and S700, according to annealing temperatures.

For the collection of the X-ray powder-diffraction (XRPD) data a Brucker D8 Advance X-ray powder diffractometer was used. The diffractometer was equipped with a Cu-tube. The generator was set-up at 40 kV and 40 mA. The divergence and receiving slits were 0.3° and 0.1 mm, respectively. The scanning range was 15–115° in 2θ, with a step of 0.05° and a scanning time of 35 s per step.

Transmission electron microscopy (TEM) images were obtained using a thermoionic 200 kV Tecnai T20 microscope operating at an accelerating voltage of 200 kV.

For electrical measurements the samples were prepared by pressing powders into tablets. A silver paste was used to connect sample with short lead copper wires in order to put the tablet into a HP-16047 A test fixture. The material was stimulated with an AC source and the actual voltage across the material was monitored. Data equivalent to the real and imaginary parts of complex electrical quantities are measured as a function of the frequency of the applied electric field by using the impedance spectroscopy technique. Impedance analyzer HP-4194A was used in the frequency range from 100 Hz to 40 MHz at three different temperatures: room temperature, 50 °C and 70 °C. A personal computer with in-house developed software tool was used for the control of the whole measurement process and for acquisition of measured data. Electrical properties reported here – resistivity, dielectric permittivity, and loss tangent were derived by knowing the geometrical dimensions of the sample tablet and by measuring its capacitance and parallel resistivity.

Magnetic measurements were performed using an MPMS XL-5 SQUID magnetometer. Magnetization vs. field, $M(H)$, was measured at room temperature up to field of 5 T. Zero-field-cooled (ZFC) and Field-cooled (FC) magnetization $M(T)$ was measured in

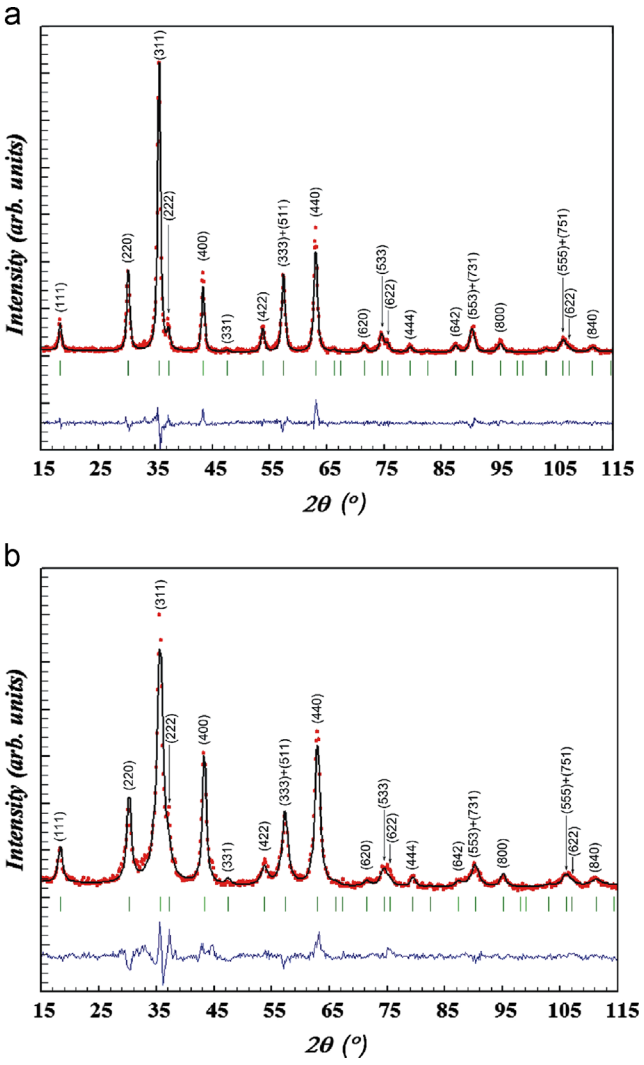

Fig. 1. Result of the Rietveld refinement for as-prepared (S0) (a) and annealed nickel ferrite (S700) (b). Dots denote observed step intensities; the line represents the corresponding calculated values. The difference curve between observed and calculated values is given at the bottom.

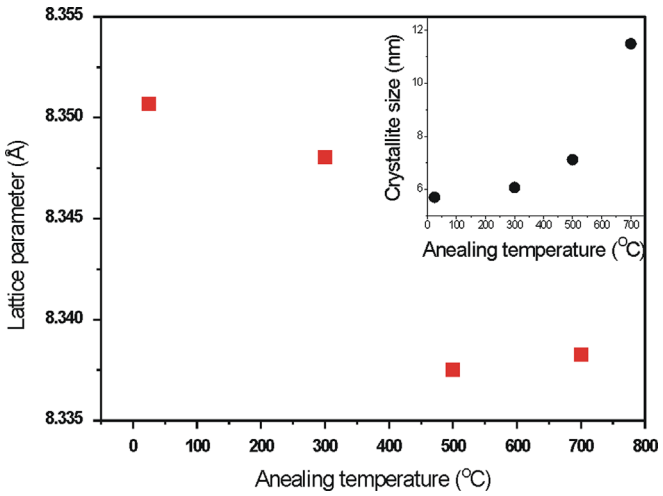

Fig. 2. Lattice parameter (main panel) and crystallite size (the inset) versus annealing temperature for Nickel ferrite nanoparticles.

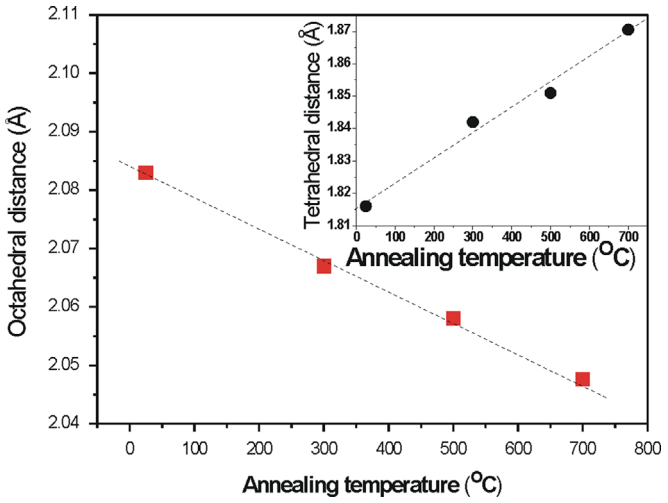

Fig. 3. Octahedral (main panel) and tetrahedral (the inset) cation–anion bond lengths change with annealing temperature for Nickel ferrite nanoparticles (lines are guide for eyes).

the temperature range of 2–300 K, and in an applied field of 100 Oe.

3. Results and discussion

3.1. Structural and microstructural analysis

The X-ray diffraction patterns of the samples were indexed in the expected $Fd\bar{3}m$ space group. Small differences in positions and peak widths denote changes of lattice parameters and microstructure (crystallite size and strain) with annealing. Collected X-ray diffraction data was used to refine atomic and crystal structure parameters by Fullprof computer program [13], such as: lattice and oxygen parameters, occupation parameters and distances between atoms as well as crystallite size and microstrain. Fig. 1 shows a good agreement between experimental data and structure model for S0 and S700 samples.

Refined values of lattice parameters of S0 and S300 were greater than value for bulk nickel ferrite ($a=8.338$ Å [14]). As could be seen from Fig. 2, lattice parameter decreases with the increase in annealing temperature, evidently approaching the bulk value. The reasons for this kind of behavior are cation redistribution between tetrahedral 8a and octahedral 16d sites in spinel type structure, polyvalence of cations, as well as crystal structure defects.

By Mossbauer spectroscopy the cation distribution in the S0 sample was found to be $(Ni_{0.34}Fe_{0.66})[Ni_{0.66}Fe_{1.34}]$ [12]. It was expected that annealing would lead to migration of nickel ions from tetrahedral to octahedral sites and induce rise in the occupation parameter of nickel in octahedral position, thus leading to bulk structure. The attempt to refine occupation parameters of cations and to determine cation distribution in annealed samples failed. Nickel and iron are second nearest neighbors in periodic system, so X-ray hardly distinguishes them, and this leads to unstable refinement of occupancies. Cation migration from site to site influences interatomic distances. Oxygen–metal distances for both octahedral and tetrahedral sites, O–B and O–A, respectively, calculated within refinement procedures are given on Fig. 3. Increase in O–A distance with the annealing temperature and vice versa for O–B distance was found. Consideration of Ni^{2+}, Fe^{3+} and Fe^{2+} ionic radii values, for both low and high spin states, pointed out that increase in O–A distance is consistent with replacement of Ni^{2+} with Fe^{2+} within tetrahedral sites ($r(Fe^{2+}) > r(Ni^{2+}) > r(Fe^{3+})$), and decrease in O–B distance is consistent with replacement of Fe^{2+} (high spin) with Ni^{2+} within octahedral sites. Hence, analysis of the interatomic distance values indicated presence of ferrous ions in the samples. Mechanochemical synthesis generally induces structure defects with small deviations from the stoichiometry, followed by oxidation/reduction of polyvalent ions. The presence of Fe from the stainless steel vial and balls can provide reducing environment, necessary to reduce small amount of Fe^{3+} to Fe^{2+}. Assuming that mechanochemical synthesis induces reduction of some ferric ions in the sample S0, then oxidation of ferrous ions during annealing could occur. The experimentally found lowering of the lattice parameter is consistent with gradual oxidation of ferrous ions with the increase in annealing temperature.

Crystallite size was obtained by line profile analysis of the X-ray diffraction data using Fullprof program. X-ray line broadening was analyzed by the refinement of regular TCH–pV function parameters (isotropic effects) [15]. Crystallite size values are shown in the inset of Fig. 2. They are nearly the same for as-prepared sample and the samples annealed up to 500 °C (5–6 nm), and is approximately two times larger for the sample annealed at 700 °C ($\approx$ 11 nm).

Transmission electron microscopy was used in order to determine particle size and their distribution and morphology. Two samples were selected for these examinations: as-prepared sample and the one annealed at 700 °C. Particles are spherical in shape and agglomerated due to magnetic interactions among them (Fig. 4). The particle size is 8–12 nm in the as-prepared

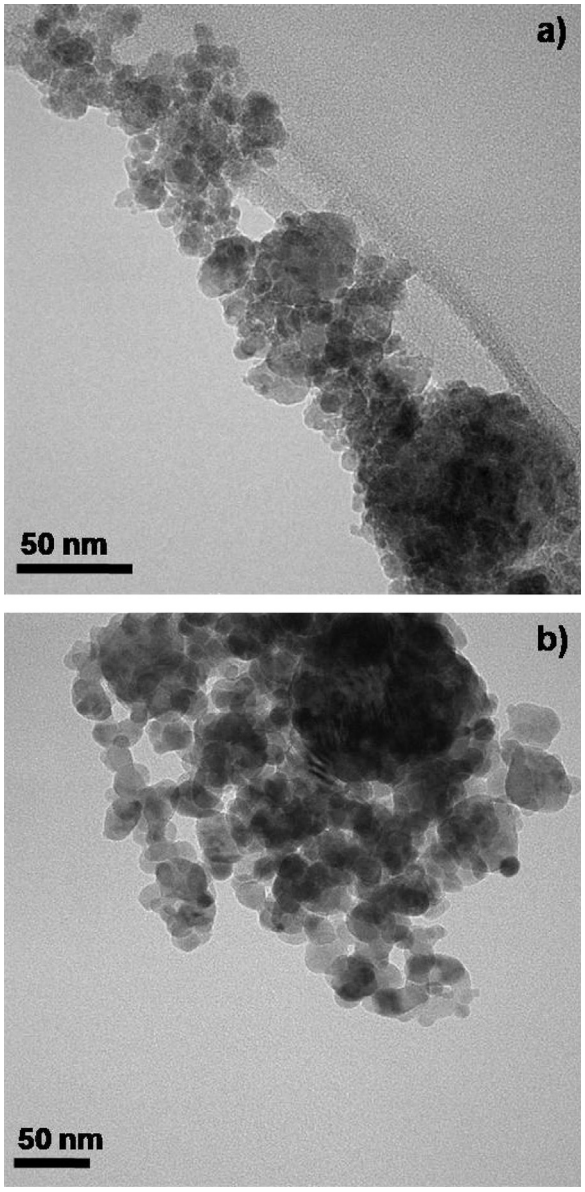

Fig. 4. TEM images of (a) as-prepared and (b) annealed at 700 °C Nickel ferrite.

sample and 15–25 nm (mostly 20 nm) in the annealed sample. Determined crystallite size from X-ray broadening analysis is smaller than particle size observed from TEM micrograph analysis. Hence, we can conclude that particles are composed from one, two or more crystallites.

3.2. Electrical properties

Variation of resistivity with frequency for investigated samples at room temperature in the range 10^3–10^6 Hz is shown in Fig. 5. The resistivity decreases with the increase of frequency in all cases in accordance with Koop's phenomenological theory [16]. The lowest resistivity was found for as-prepared sample, S0 and increases with the increase of the crystallite size. To explain this result we should take in consideration differences between samples

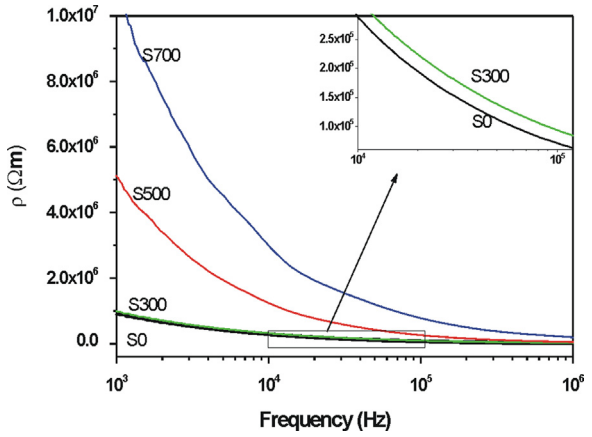

Fig. 5. Frequency dependence of electrical resistivity for Nickel ferrite nanoparticles.

in two aspects: (i) cation distribution within two non-equivalent spinel sites and (ii) concentration of ferrous ions. Concerning ion distribution, annealing process was expected to result in migration of iron ions from octahedral to tetrahedral sites. Then, decrease of iron concentration in octahedral sites decreases probability of hopping of electrons between Fe^{2+} and Fe^{3+} ions resulting in resistance increase. Concentration of ferrous ions was concluded to be the highest in the sample S0 and decreases with the increase of samples crystallite size. Ferrous ions act as donors in investigated materials, and decreasing of their concentration influences increasing of resistivity.

Literature data on resistivity of nanosize nickel ferrites pointed out its maximum at 100 °C [17] or at 105 °C [18]. It seems that interesting phenomena in nickel ferrite nanoparticles occur above room temperature. Consequently, we investigated variation of resistivity with frequency at selected temperatures, 25 °C, 50 °C and 70 °C. For samples S0, S300 and S500 resistivity has the highest value at temperature of 50 °C, Fig. 6. It is worth mentioning the work of Younas et al. [19] where resistivity was the lowest around 85 °C, because of semiconductor to metal transition in sol–gel synthesized $NiFe_2O_4$. We will briefly discus observed results. Conductivity of a material is determined by the concentration of free carriers and their mobility [20]. It is also known that after most of the donors have lost their carriers the resistance starts to increase slightly due to the reduced carriers' mobility (as in metals). Obviously, the measurements were started in this region and resistivity of samples S0, S300 and S500 increased slightly in the temperature region up to 50 °C. This so called saturation region exists up to the temperature where thermally generated intrinsic carriers occur. Their concentration increases with temperature and at one point resistivity starts to decrease. The resistivity values measured at temperature 70 °C were lower than at 50 °C. So, it can be concluded that at one point in the temperature region from 50 °C to 70 °C concentrations of thermally generated intrinsic carriers became high enough to overcome effect of reduced mobility. Sample S700 behaved like intrinsic semiconductor, its resistivity decreased with the increase of temperature.

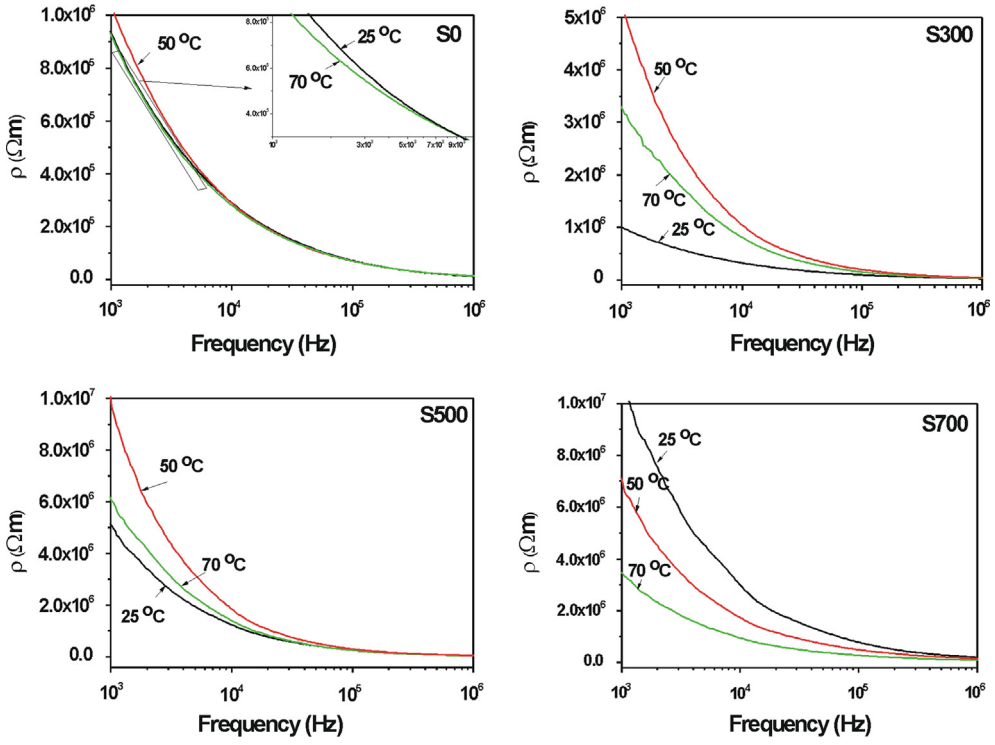

Fig. 6. Frequency dependence of electrical resistivity for Nickel ferrite nanoparticles measured at different temperatures (see text).

The variation of the real part of the dielectric constant with frequency at room temperature is depicted in Fig. 7(a). It decreases continuously with the increase of frequency. For samples S300, S500 and S700 the decreasing trend becomes slower as the frequency increases. Dielectric constant is size dependent as can be seen in Fig. 7(a). It decreases with the increase of crystallite size for samples whose average crystallites were smaller than 8 nm. Papers referred to nanosize nickel ferrite report that crystallite size increase was followed by both decrease [21] and increase [22] of dielectric constant. The model proposed by Tian et al. [23] predicts a decrease or an increase in dielectric constants with decrease of particle diameter depending on interface conditions and shape of nanocrystals.

The variation of dielectric loss tangent with frequency at room temperature is presented in Fig. 7(b). It can be seen that dielectric loss tangent decreases with the increase in frequency as expected for ferrites. The other important observation is that the loss is size dependent. It decreases with the increase in size, except for sample S300. In comparison with nickel ferrite prepared by the sol–gel method [18] loss tangent values are lower. The low value of dielectric loss indicates that the investigated samples are suitable for high-frequency applications.

3.3. Magnetization versus temperature and field

Temperature dependencies of ZFC and FC magnetization for as-prepared sample, S0, are shown in Fig. 8. The ZFC and FC magnetization curves furcate at the maximum temperature of measurements, 300 K. Temperature of maximum in ZFC branch T_{max} is close to 300 K. The appearance of a maximum in ZFC magnetization is typical for a superparamagnetic (SPM) behavior or super spin glasses (SSGs), where T_{max} is the corresponding blocking temperature, T_B, or frizzing temperature, T_{SG}. A broad maximum in ZFC branch is a consequence of a broad particle size distribution, as was shown by TEM examinations (Fig. 4). In the FC branches magnetization increases a little bit from room temperature to 200 K, and below it shows a tendency to be saturated. For SPM systems below T_B a constant increase in the FC magnetization with the temperature decrease is present [24]. In contrast, for SSG systems below T_{SG} flatness or even decrease in FC magnetization is usually noticed. The found FC behavior indicates the inter-particle interactions and probably a spins glass state.

The hysteresis loops of the samples, recorded at 300 K, are shown in Fig. 9. One of the remarkable features of the magnetization curves is their increase with applied field and the absence of saturation even in the field of 5 T (maximum field strength achievable on XL-5 SQUID magnetometer). The observed behavior should be mainly addressed to the canting of spins in the ferrimagnetically ordered particle core due to strong A–B superexchange interactions [1]. Nevertheless, the non-saturation can be also an indication of presence of spin disorder at the particle surface [1]. The M_S value has been estimated by extrapolation of the M vs. $1/H$ curve when $1/H \rightarrow 0$. Sample S700 has the highest saturation magnetization ($M_S = 36.5$ emu/g) while sample S300 has the smallest value (33 emu/g). Annealing at 500 °C induced a decrease of M_S in sample S500 ($M_S = 35$ emu/g). Obtained M_S value for as-prepared sample was 36 emu/g and smaller than value for bulk and ultrafine Nickel ferrite (about 50 emu/g [25,26]). Besides thermal annealing, magnetic properties of nickel ferrite nanoparticle can be tuned

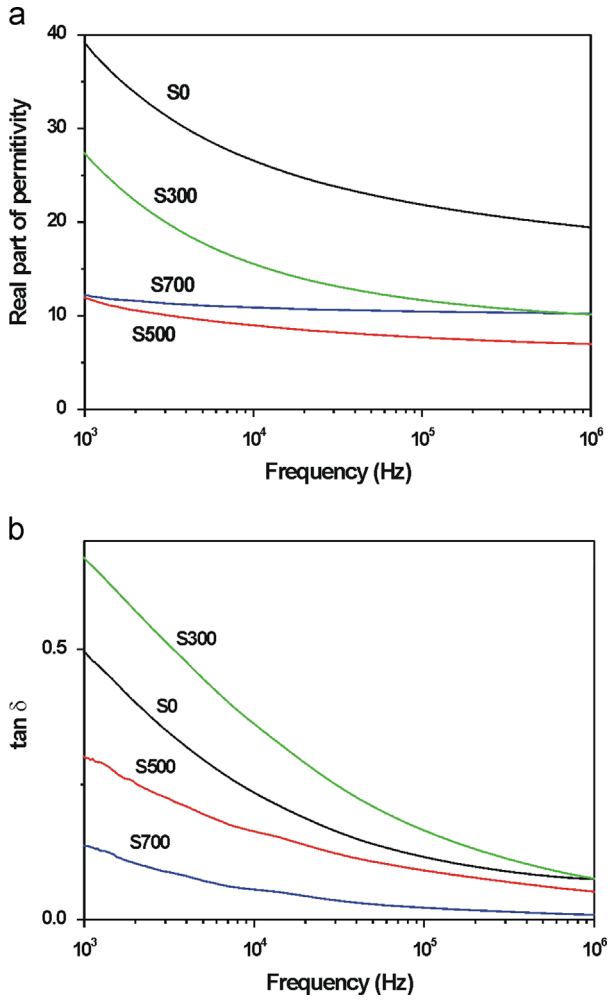

Fig. 7. (a) Variation with frequency of the real part of the dielectric constant and (b) dielectric loss tangent (tan δ) as a function of frequency for Nickel ferrite nanoparticles.

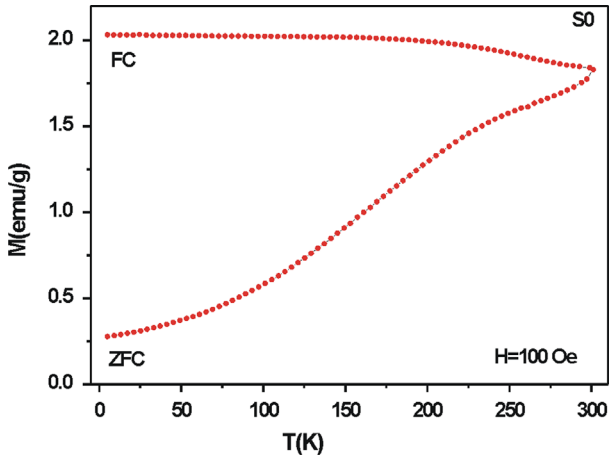

Fig. 8. ZFC–FC magnetization versus temperature for as-prepared Nickel ferrite (S0).

by doping [27]. The coercitivities, H_C were found to be: 190 Oe (S0), 120 Oe (S300), 165 Oe (S500) and 170 Oe (S700). Many factors have an influence on the values of M_S and H_C, such as:

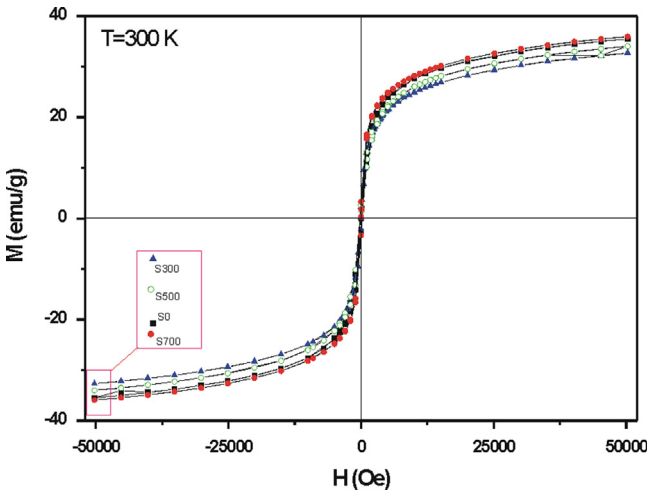

Fig. 9. Hysteresis loops of the samples S0, S300, S500 and S700 at 300 K.

crystallite size, microstrain, cation distribution, presence of parasitic phases, etc. Also, magnetic properties are strongly influenced by surface, magnetocrystalline and shape anisotropies. Additionally, magnetic disorder exists around defects in the interior of the particles and has a contribution to the net value.

4. Conclusion

Evolution of (micro)structural, magnetic, and electric properties of Nickel ferrite nanoparticles, prepared via soft mechanochemistry exposed to further thermal annealing/heating, was assessed in detail, and correlation of these properties explored. Comparative analysis of TEM micrographs and results of X-ray line broadening analysis showed significant presence of particles composed of approximately two or more crystallites. Variation of lattice parameter and octahedral and tetrahedral cation–anion bond lengths with crystallite size is a consequence of mechanochemically induced nonstoichiometry, crystal structure defects, cations polyvalence, as well as of cation redistribution between tetrahedral and octahedral sites. Ac resistivity of Nickel ferrite nanoparticles increases with crystallite size and it was the highest for sample annealed at 700 °C. Magnetic investigations indicate the existence of the interaction among ferrite nanoparticles. Saturation magnetization of as-prepared sample is about 30% smaller than value for bulk nickel ferrite. Magnetic properties are under influence of different factors and it is not possible to determine contribution of each of them.

Acknowledgment

The Serbian Ministry of Science, Technology and Development supported this work financially, project Grants no. III45015. We are thankful to Dr. Pilar Catalayed for performing TEM measurements.

References

[1] B. Antić, A. Kremenović, L. Bessais, J. Blanuša, M. Perović, P. Vulić, V. Spasojević, E.S. Božin, An integrated study of thermal treatment effects on the microstructure and magnetic properties of Zn-ferrite nanoparticles, Journal of Physics: Condensed Matter 25 (2013) (086001 (13 pp).

[2] S.K. Pradhan, S. Bidb, M. Gateshki, V. Petkov, Microstructure characterization and cation distribution of nanocrystalline magnesium ferrite prepared by ball milling, Materials Chemistry and Physics 93 (2005) 224–230.

[3] D. Carta, M.F. Casula, A. Falqui, D. Loche, G. Mountjoy, C. Sangregorio, A. Corrias, A structural and magnetic investigation of the inversion degree in ferrite nanocrystals MFe_2O_4 (M=Mn, Co, Ni), Journal of Physical Chemistry C 113 (2009) 8606–8615.

[4] S.S. Ata-Allah, M. Kaiser, Semiconductor-to-metallic transition in Cu-substituted Ni–Mn ferrite, Physica Status Solidi 201 (2004) 3157–3165.

[5] N.F. Mott, R. Peierls, Discussion of the paper by De Boer and Verwey, Proceedings of the Physical Society, London 49 (1937) 72–76.

[6] J. Liu, H. He, X. Jin, Z. Hao, Z. Hu, Synthesis of nanosized nickel ferrites by shock waves and their magnetic properties, Materials Research Bulletin 36 (2001) 2357–2363.

[7] B.P. Jacob, A. Kumar, R.P. Pant, S. Singh, E.M. Mohamed, Influence of preparation method on structural and magnetic properties of nickel ferrite nanoparticles, Bulletin of Materials Science 34 (2011) 1345–1350.

[8] H. Lord, R. Parker, Electrical resistivity of nickel ferrite, Nature 188 (1960) 929–930.

[9] J. Jacob, M.A. Khadar, Investigation of mixed spinel structure of nanostructured nickel ferrite, Journal of Applied Physics 107 (2010) (114310 (10 pp).

[10] R.J. Brook, W.D. Kingery, Nickel ferrite thin films: microstructures and magnetic properties, Journal of Applied Physics 38 (1967) (3589 (6 pp).

[11] A.S. Nikolić, N. Jović, J. Rogan, A. Kremenović, M. Ristić, A. Meden, B. Antić, Carboxylic acids and polyethylene glycol assisted synthesis of nanocrystalline nickel ferrites, Ceramics International 39 (2013) 6681–6688.

[12] Z.Ž. Lazarević, Č. Jovalekić, A. Rečnik, V.N. Ivanovski, A. Milutinović, M. Romčević, M.B. Pavlović, B. Cekić, N.Ž. Romčević, Preparation and characterization of spinel nickel ferrite obtained by the soft mechanochemically assisted synthesis, Materials Research Bulletin 48 (2013) 404–415.

[13] J. Rodriguez-Carvajal, FullProf Computer Program, http://www.ill.eu/sites/fullprof/.

[14] K.N. Subramanyam, Neutron and X-ray diffraction studies of certain doped nickel ferrites, Journal of Physics C: Solid State Physics 4 (1971) 2266–2268.

[15] V. Honkimäki, P. Surotti, Effects of instrument function, crystallite size, and strain on reflection profiles, in: R.L. Snyder, J. Fiala, H.J. Bunge (Eds.), Defect and Microstructure Analysis by Diffraction, Oxford University Press, New York, 1999, pp. 41–58.

[16] C.G. Koops, On the dispersion of resistivity and dielectric constant of some semiconductors at audiofrequencies, Physical Review 83 (1951) 121–124.

[17] A.M. Bhavikatti, S. Kulkarni, A. Lagashetty, Electromagnetic studies of Nickel ferrite synthesized by microwave route, International Journal of Engineering Science and Technology 3 (2011) 687–695.

[18] A.B. Rajput, S. Hazra, N.B. Krishna, P. Chavali, S. Datla, N.N. Ghosh, Preparation of $NiFe_2O_4$ nanopowder via EDTA precursor and study of its properties, Particuology 10 (2012) 29–34.

[19] M. Younas, M. Nadeem, M. Atif, R. Grossinger, Metal-semiconductor transition in $NiFe_2O_4$ nanoparticles due to reverse cationic distribution by impedance spectroscopy, Journal of Applied Physics 109 (2011) (093704 (8 pp).

[20] R.L. Petritz, Theory of an experiment for measuring the mobility and density of carriers in the space–charge region of a semiconductor surface, Physical Review 110 (1958) 1254–1262.

[21] L. Li, Z. Jian-Ping, L. Qian, Z. Gangqiang, C. Xian-Zhi, B. Xiao-Bing, L. Peng, Grain size effect on the dielectric and magnetic properties of $NiFe_2O_4$ ceramics, Physica E 43 (2011) 1798–1803.

[22] S. Singh, N.K. Ralhan, R.K. Kotnala, K.C. Verma, Nanosize dependent electrical and magnetic properties of $NiFe_2O_4$ ferrite, Indian Journal of pure & Applied Physics 50 (2012) 739–743.

[23] M. Tian, M. Li, J.C. Li, Effect of size on dielectric constant for low dimension materials, Physica B 406 (2011) 541–544.

[24] V. Spasojevic, A. Markovic, M. Perovic, V. Kusigerski, J. Blanusa, Superspin-glass like behavior of nanoparticle $La_{0.7}Ca_{0.3}MnO_3$ obtained by mechanochemical milling, Journal of Nanoparticle Research 13 (2011) 763–771 (and references therein).

[25] P. Sivakumar, R. Ramesh, A. Ramanand, S. Ponnusamy, C. Muthamizhchelvan, Synthesis and characterization of nickel ferrite magnetic nanoparticles, Materials Research Bulletin 46 (2011) 2208–2211.

[26] Z. Zhang, Y. Liu, G. Yao, G. Zu, D. Wu, Y. Hao, Synthesis and characterization of dense and fine nickel ferrite ceramics through two-step sintering, Ceramics International 38 (2012) 3343–3350.

[27] N.M. Deraz, Effects of magnesia addition on structural, morphological and magnetic properties of nano-crystalline nickel ferrite system, Ceramics International 38 (2012) 511–516.